FULL PAPER

ADVANCED FUNCTIONAL MATERIALS

Architectural Control of Hierarchical Nanobelt Superstructures in Catanionic Reverse Micelles**

By *Hongtao Shi*, *Limin Qi*,* *Jiming Ma*, and *Nianzu Wu*

$BaXO_4$ (X = Mo, W) nanobelts and a variety of hierarchical superstructures assembled from the nanobelts have been synthesized in a catanionic reverse-micelle system. The effects of various factors, such as the mixing ratio (r) between the anionic and cationic surfactants, the temperature, and the presence of polymeric additives, on the formation of the nanobelts and their hierarchical assembly have been examined in detail. In particular, r has been shown to be powerful in modulating the formation and assembly of the $BaMoO_4$ and $BaWO_4$ nanobelts. Architectural control of the penniform nanobelt superstructures has been readily achieved by changing the experimental parameters. A plausible two-stage growth mechanism has been proposed for the formation of penniform $BaXO_4$ nanobelt superstructures in catanionic reverse micelles.

1. Introduction

One-dimensional (1D) nanostructures, such as nanotubes, nanowires, nanorods, and nanobelts, have stimulated intensive interest due to their importance in fundamental research and potential application in the fabrication of nanoscale devices.[1] Many recent efforts have been focused on the hierarchical assembly of 1D nanoscale building blocks into ordered superstructures or complex architectures, which is a crucial step towards the realization of functional nanosystems and would offer opportunities to explore their novel collective optical, magnetic, and electronic properties.[2–5] For example, ordered nanorod/nanowire arrays have been obtained by the self-assembly of preformed uniform nanorods,[2,6,7] or the direct growth of nanowire arrays on solid templates.[8] Notably, the self-organized crystal growth of novel hierarchical architectures made of nanorods/nanowires has been achieved via two different routes. The chemical vapor deposition method has been employed to fabricate a variety of branched nanowire structures; examples include ZnO nanobridges, nanonails, and nanocombs.[9] On the other hand, the solution synthesis of complex nanorod/nanowire superstructures, such as multi-armed,[3,10] multiple cone-shaped,[11] penniform,[12] and snowflake-like nanostructures,[13] has advanced greatly in recent years. As a new family of 1D nanostructures, nanobelts have received much attention because of their unique properties and potential applications in building functional nanodevices;[14,15] however, there has only been limited success in assembling nanobelts into hierarchical architectures.[16] It remains a significant challenge to develop facile methods for the fabrication and architectural control of hierarchical nanobelt superstructures.

It has been well known that reverse micelles and microemulsions can be used as soft colloidal templates for controlling the size and shape of inorganic nanocrystals.[17] Specifically, inorganic nanorods/nanowires of various materials including metals,[18] semiconductors,[19] as well as barium-containing compounds have been successfully synthesized in reverse-micelle media.[2,20] Although mixed surfactants have been widely used as capping reagents, showing different surface-selectivities for the solution synthesis of 1D nanostructures,[21] the use of reverse micelles formed by mixed surfactants as nanostructured media for the controlled synthesis of 1D nanostructures has not been achieved until recently.[22] In our recent communications, an unique catanionic reverse-micelle system formed by mixed cationic–anionic surfactants has been employed for the synthesis of $BaWO_4$ nanowires,[22] and their hierarchical assembly into penniform superstructures under the direction of a block copolymer.[12] Interestingly, novel $BaCrO_4$ nanobelts and their tree-like superstructures have been successfully produced in the catanionic reverse micelles by simply changing the molar ratio (r) between the mixed anionic and cationic surfactants.[23] This result has led us to explore the potential applications of the catanionic reverse-micelle system in the synthesis of barium molybdate/tungstate nanobelts as well as their hierarchical superstructures. Recently, the synthesis of 1D metal molybdate and tungstate materials has attracted much attention owing to their potential wide-ranging applications.[15,20d,24] Specifically, $BaXO_4$ (X = Mo, W) crystals with a scheelite structure are important photo-electronic materials and are useful for designing all-solid-state lasers.[25] In this work, a systematic examination of the synthesis of $BaXO_4$ nanobelts and their self-assembly into complex architectures in catanionic reverse micelles is presented. It has been shown that architectural control of hierarchical nanobelt superstructures can be readily achieved by changing the experimental parameters.

[*] Prof. L. Qi, H. Shi, Prof. J. Ma, Prof. N. Wu
State Key Laboratory for Structural Chemistry of Unstable and Stable Species
College of Chemistry, Peking University
Beijing 100871 (P.R. China)
E-mail: liminqi@chem.pku.edu.cn

[**] This work was supported by NSFC (20325312, 20473003, 20233010) and FANEDD (200020). We thank Prof. Humin Cheng for valuable discussions and Hongtao Shi thanks Prof. Buyao Zhu for helpful instruction.

  DOI: 10.1002/adfm.200400242

ADVANCED FUNCTIONAL MATERIALS

2. Results and Discussion

2.1. Phase Regions of Catanionic Reverse Micelles

The model shown in Scheme 1 illustrates the conceivable structure of catanionic reverse micelles at different mixing ratios (r) between anionic and cationic surfactants. When $r = 1$, the mixed surfactant film stays in a tight state. If anionic and catanionic surfactants are mixed in non-equimolar ratios, i.e., $r > 1$ or $r < 1$, the mixed surfactant monolayer would become looser because of the electrostatic repelling force between the ionic heads of the excess surfactant molecules. The selected catanionic reverse-micelle system consists of water, decane, and a mixture of two surfactants: undecylic acid and decyl amine, where the cationic surfactant was produced by the protonation of the amine by undecylic acid. Figure 1 presents phase diagrams of the undecylic acid–decyl amine/decane/water system, which suggests that the reverse micellar phase (L_2) area in the phase diagram is basically similar to the L_2 area reported for the undecenoic acid–decyl amine/decane/water system.[26] As shown in Figure 1a, the mixing ratio r considerably affects the L_2 area and relatively more pronounced changes are observed for $r > 1$, which could be partly attributed to the difference in the interactions between different surfactant molecules with different headgroups and hydrocarbon chain lengths. When the temperature is increased from 30 to 50 °C, the reverse-micelle region extends toward higher surfactant-mixture contents, and also the region moves away slightly from the water apex. This result is essentially consistent with the result obtained from the catanionic octylammonium octanoate/octane/water system, where the enlarged L_2 area at higher temperatures has been attributed to the higher degree of conformational freedom for the hydrocarbon chains in the reverse-micelle structure compared with the packing in a lamellar bilayer.[27] It is noted that the temperature would affect many factors, such as the dissociation of undecylic acid and the protonation of decyl amine, the solubility of the surfactants in oil, and the electrostatic interaction between the surfactant headgroups, which suggests that the actual situation could be even more complex. Nevertheless, the obtained results indicate that the surfactant mixing ratio as well as the temperature largely influences the phase region as well as the microstructure of the catanionic reverse micelles, which are expected to play a key role in the controlled synthesis and hierarchical assembly of 1D nanostructures.

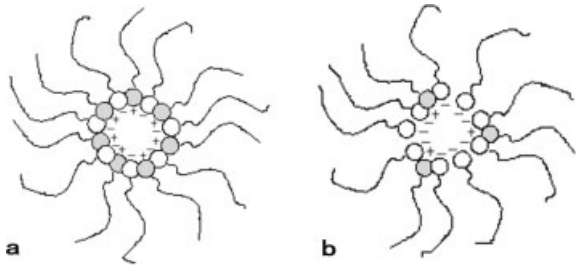

Scheme 1. Schematic diagram of catanionic reverse micelles: a) $r = 1$, b) $r > 1$.

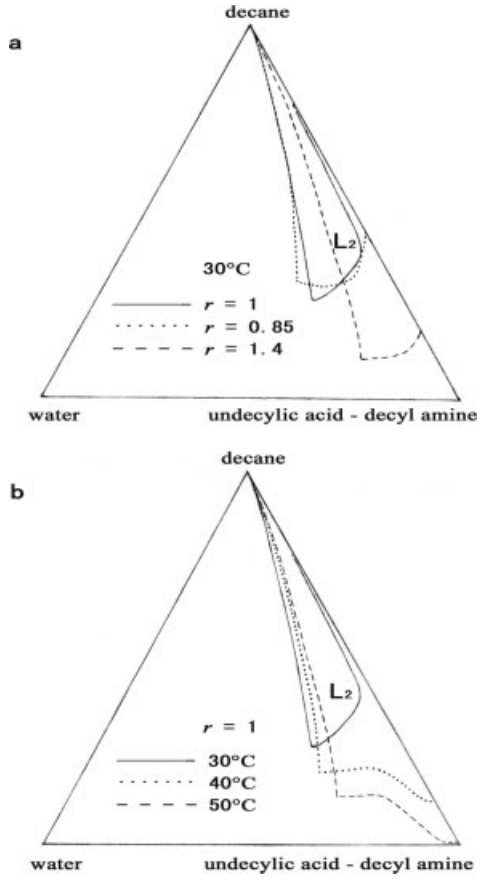

Figure 1. Phase diagrams of the mixed system of undecylic acid–decyl amine/decane/water with indicated a) the reverse micellar phase (L_2) at different values of r (the mixing ratio between undecylic acid and decyl amine) and b) the L_2 phase at different temperatures for $r = 1$.

2.2. $BaMoO_4$ Nanostructures

The synthesis of $BaMoO_4$ nanostructures was simply achieved by the reaction between Ba^{2+} ions and MoO_4^{2-} ions solubilized in the catanionic reverse micelles. Figure 2 shows typical transmission electron microscopy (TEM) and high-resolution TEM (HRTEM) images of the $BaMoO_4$ nanobelts obtained at a mixing ratio $r = 1$, i.e., in the presence of equimolar undecylic acid and decyl amine. At 50 °C, bundles of $BaMoO_4$ nanobelts with lengths up to several tens of micrometers, widths of ~10 nm, and thickness of ~3 nm were obtained (Figs. 2a,b). The electron diffraction (ED) pattern corresponding to the two nearly parallel, straight nanobelts exhibited diffraction spots predominantly corresponding to the [010] zone of the tetragonal $BaMoO_4$ structure with (00L) spots along the length direction, indicating that each nanobelt was a single crystal with the c axis along the length direction and the a axis along the width direction. The HRTEM image shown in

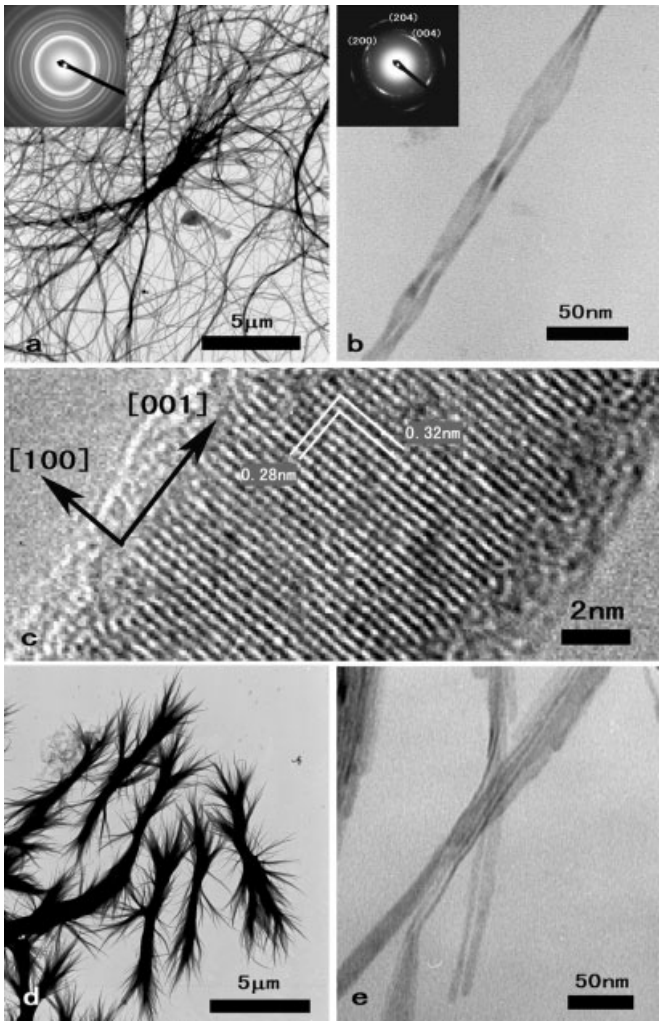

Figure 2. a,b,d,e) TEM and c) HRTEM images of $BaMoO_4$ nanobelts formed at $r = 1$, and 50 °C (a–c) and 30 °C (d,e). $[BaMoO_4] = 0.05$ mol L^{-1}. Insets show the corresponding ED patterns.

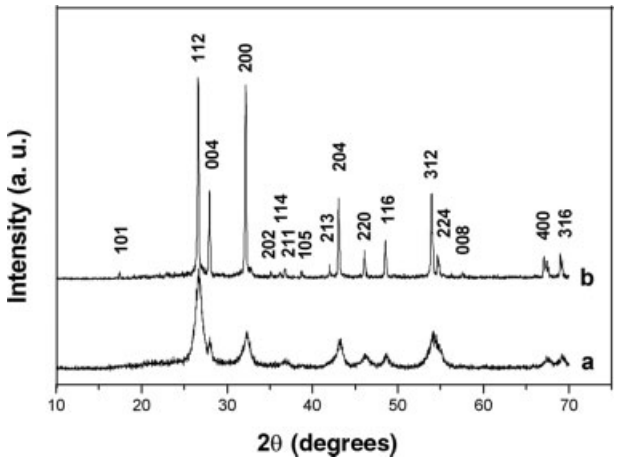

Figure 3. XRD patterns of $BaMoO_4$ nanostructures formed at a) $r = 1$ and b) $r = 1.5$, at 50 °C. $[BaMoO_4] = 0.05$ mol L^{-1}.

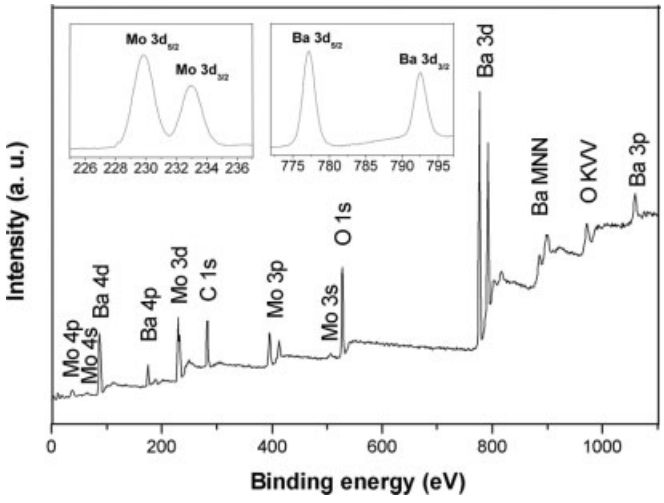

Figure 4. XPS spectra of $BaMoO_4$ nanobelts formed at $r = 1$ and 50 °C. $[BaMoO_4] = 0.05$ mol L^{-1}.

Figure 2c exhibited clear (100) and (001) fringes, confirming that the single-crystalline nanobelt was enclosed by top surfaces of ±(100), and side surfaces of ±(010). The related X-ray diffraction (XRD) pattern (Fig. 3a) together with the X-ray photoelectron spectroscopy (XPS) spectra (Fig. 4) provide evidence that the nanobelt bundles were pure $BaMoO_4$ crystals of a tetragonal scheelite structure (Joint Committee on Powder Diffraction Standards (JCPDS) card 29-0193: $a = 0.558$ nm, $c = 1.282$ nm). The broadening of the XRD peaks resulted from the small thickness and width of the nanobelts. When the reaction temperature was decreased to 30 °C, similar bundles of $BaMoO_4$ nanobelts with widths of about 10 nm and a thickness of ~3 nm were also obtained, although the nanobelt length was decreased to ~10 μm (Figs. 2d,e). This tendency for the variation of the nanobelt length with temperature is similar to that for 1D $BaWO_4$ nanostructures obtained in the same reverse-micelle system at $r = 1$; however, $BaMoO_4$ nanobelts rather than nanowires were obtained here, which was in contrast to the $BaWO_4$ nanowires obtained previously.[22]

Figure 5 presents typical TEM images of the $BaMoO_4$ nanostructures obtained at a mixing ratio far below 1 ($r = 0.3$) and at a mixing ratio slightly larger than 1 ($r = 1.3$), which suggested that $BaMoO_4$ nanobelts similar to those obtained at $r = 1$ were always obtained whether the reaction was carried out at 50 °C or 30 °C. However, a further increase in the mixing ratio resulted in a significant change in the architecture of the $BaMoO_4$ nanostructures. At 50 °C, when r was increased to 1.5, unusual penniform $BaMoO_4$ nanostructures with nanobelts grown on both sides of each shaft with an angle of ~50° were obtained (Fig. 6). The related ED pattern suggested that the shaft was grown along the [204] direction and the length direction of each nanobelt grown on the shaft was also along the [001] direction. The corresponding XRD pattern (Fig. 3b) indicated that the penniform nanostructures including the main shafts and the side nanobelts were pure $BaMoO_4$ crystals of the tetragonal scheelite structure. As the size of the shaft was

ADVANCED FUNCTIONAL MATERIALS

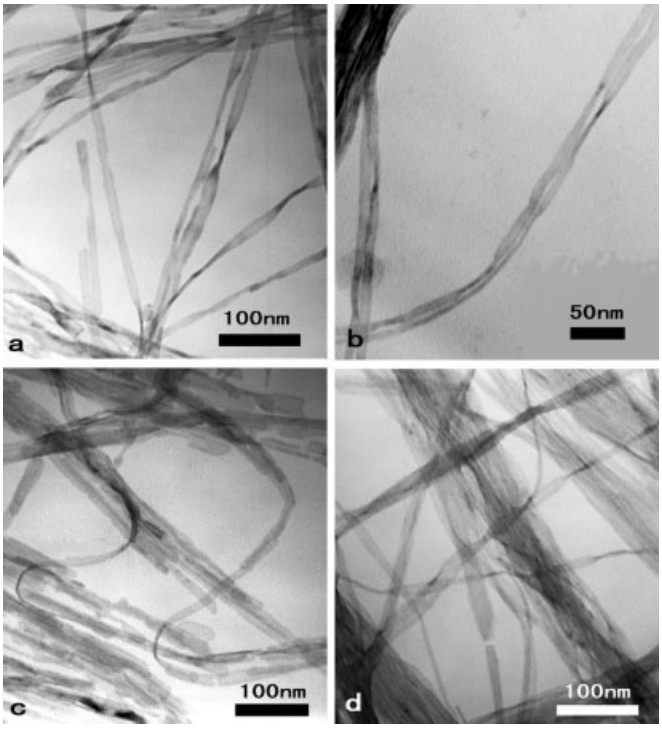

Figure 5. TEM images of $BaMoO_4$ nanobelts formed at a,b) 50 °C and c,d) 30 °C. a,c) $r = 0.3$. b,d) $r = 1.3$. $[BaMoO_4] = 0.05$ mol L^{-1}.

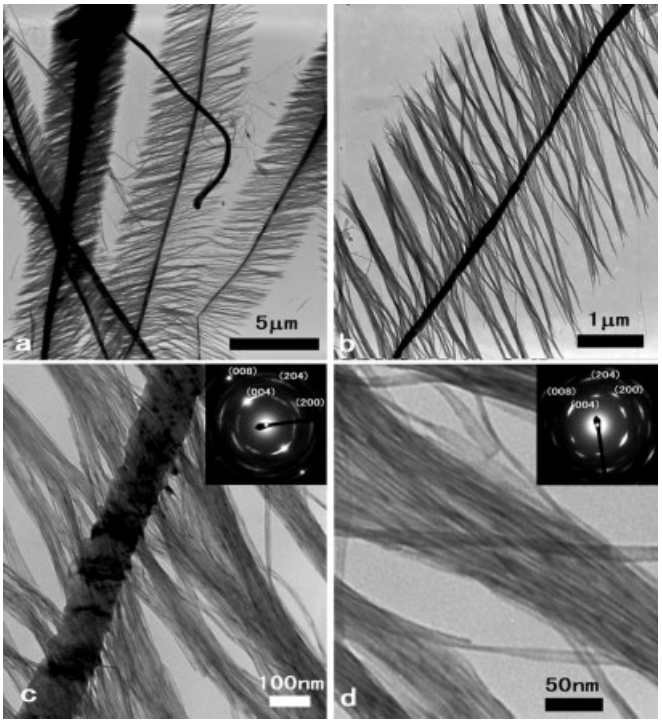

Figure 6. TEM images of $BaMoO_4$ nanostructures formed at $r = 1.5$ and 50 °C at different magnifications. $[BaMoO_4] = 0.05$ mol L^{-1}. Insets show the corresponding ED patterns.

almost beyond nanoscale dimensions (larger than 100 nm), the peaks in the XRD pattern were not broadened. Such hierarchical nanobelt superstructures are in good contrast to the penniform $BaWO_4$ nanostructures, consisting of $BaWO_4$ nanowires grown perpendicularly on both sides of the shaft, which were previously produced in the catanionic reverse-micelle system at $r = 1$, under the direction of the block copolymer poly(ethylene glycol)-*block*-poly(methacrylic acid) (PEG-*b*-PMAA).[12] If r was further increased to 1.7, bare $BaMoO_4$ shafts without side nanobelts were obtained (Fig. 7). The related ED pattern indicated that the bare shafts were $BaMoO_4$ crystals grown along the [204] direction, just the same as the growth direction of the shafts carrying side nanobelts shown in Figure 6.

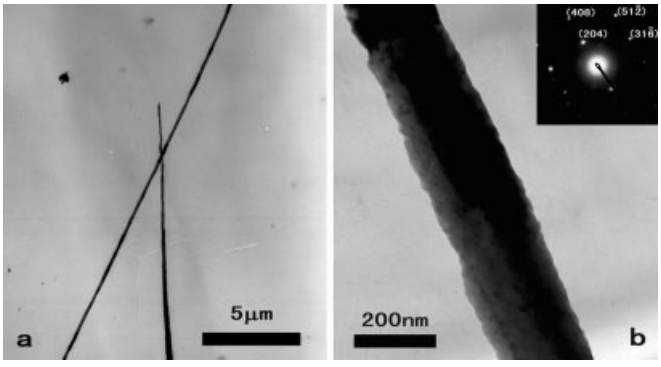

Figure 7. TEM images of $BaMoO_4$ nanostructures formed at $r = 1.7$ and 50 °C. $[BaMoO_4] = 0.05$ mol L^{-1}. Inset shows the corresponding ED pattern.

The decrease of the reaction temperature from 50 °C to 30 °C led to significant architectural modification of the penniform superstructures of $BaMoO_4$ nanobelts (Fig. 8). At $r = 1.5$, penniform $BaMoO_4$ nanostructures consisting of $BaMoO_4$ nanobelts grown perpendicularly on both sides of a slightly branched shaft were produced (Figs. 8a–c). Interestingly, the related ED patterns suggested that the shafts were grown along the [100] direction rather than the [204] direction, although the side nanobelts were still grown along the [001] direction. If r was further increased to 1.7, slightly branched bare $BaMoO_4$ shafts grown along the [100] direction were obtained (Fig. 8d), confirming the difference in the growth direction of the shafts constituting the penniform $BaMoO_4$ nanostructures obtained at two different temperatures.

For comparison purpose, the effect of the polymer PEG-*b*-PMAA on the synthesis of $BaMoO_4$ nanostructures in catanionic reverse micelles at $r = 1$ and 50 °C was also examined. As shown in Figure 9, penniform $BaMoO_4$ nanostructures consisting of [001]-oriented $BaMoO_4$ nanobelts grown perpendicularly on both sides of a smooth, [100]-oriented $BaMoO_4$ shaft were produced. It is noted the shaft was not branched, looking like the smooth shaft of the penniform $BaWO_4$ nanowire superstructures obtained at $r = 1$ and 50 °C in the presence of

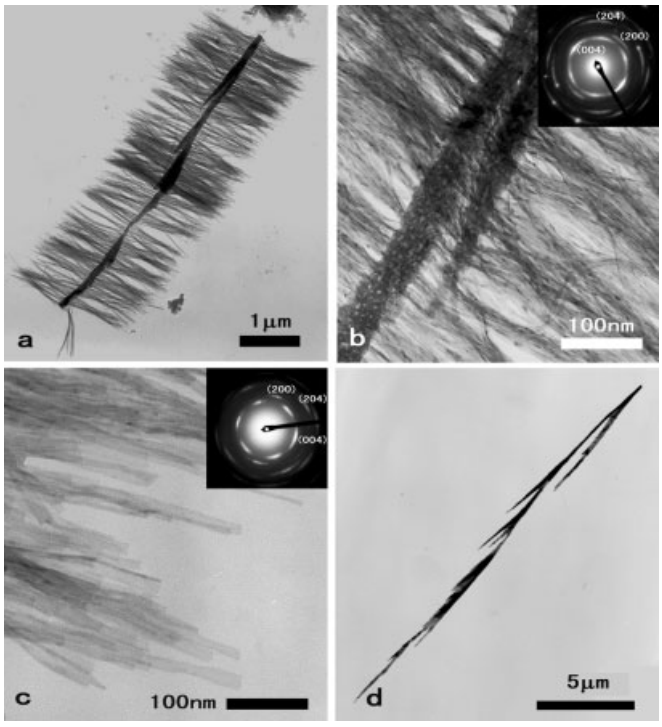

Figure 8. TEM images of $BaMoO_4$ nanostructures formed at a,b,c) $r = 1.5$ and d) $r = 1.7$ at 30 °C. $[BaMoO_4] = 0.05$ mol L^{-1}. Insets show the corresponding ED patterns.

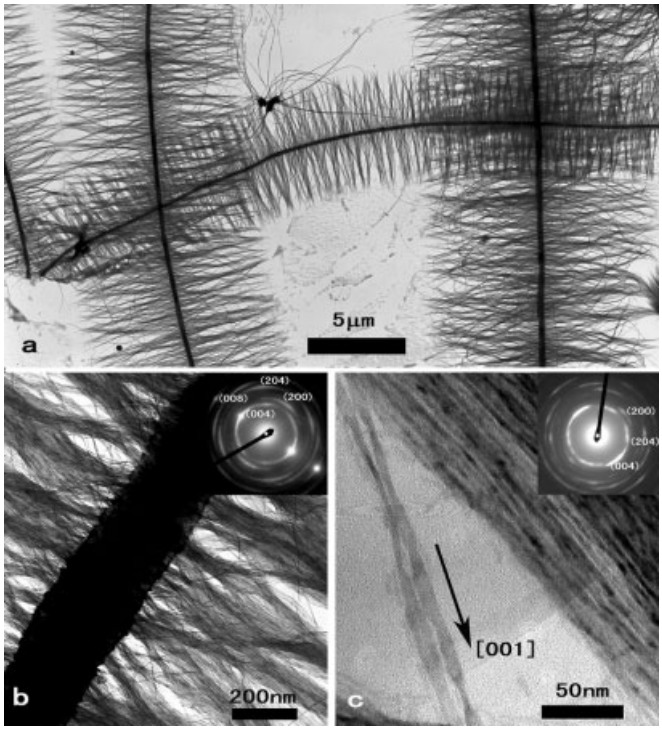

Figure 9. TEM images at various magnifications of $BaMoO_4$ nanostructures formed at $r = 1$ and 50 °C, in the presence of PEG-*b*-PMAA. $[BaMoO_4] = 0.04$ mol L^{-1}, [PEG-*b*-PMAA] = 0.6 mol L^{-1}. Insets show the corresponding ED patterns.

PEG-*b*-PMAA.[12] It also indicated that at $r = 1$, $BaMoO_4$ had a strong tendency to form nanobelts, whereas $BaWO_4$ tended to form nanowires.

Recently, a two-stage growth mechanism based on the key role of the mixed surfactant film and the selective adsorption of mixed surfactants on the growing crystals has been proposed for the formation of tree-like superstructures of $BaCrO_4$ nanobelts in catanionic reverse micelles at $r = 1.7$.[23] It was expected that such a mechanism would also be applicable to the current synthesis of hierarchical $BaMoO_4$ nanobelt superstructures after the inherent growth nature of $BaMoO_4$ crystals was taken into account. It was reasonably assumed that the interfacial surfactant film would become looser if there was excess undecylic acid in the mixed surfactant film, and so the interfacial surfactant film with varied r values would selectively bind to specific facets of $BaMoO_4$ crystals, inducing preferential crystal growth. Similar to the case of $BaCrO_4$, the $BaMoO_4$ crystal surface could preferentially adsorb undecylic acid in the mixed surfactants due to the coordination interaction between carboxylate groups and the Ba^{2+} ions, leading to a decrease in the proportion of undecylic acid in the remaining mixed surfactant film of the reverse micelles, i.e., a smaller r value.

When r was less than 1.5, the mixed surfactants could be selectively absorbed on the {100} faces of the $BaMoO_4$ crystals. Although there are four equivalent {100} faces for $BaMoO_4$ crystals with the tetragonal structure, the initial, unstable crystal nuclei could show some fluctuation in shape and might randomly adopt an uneven growth for the four {100} faces, e.g., two parallel ±(100) faces grow faster than two parallel ±(010) faces. The uneven growth of two pairs of parallel surfaces could somehow be strengthened in the crystal growth stage by the catanionic surfactants, which were supposed to bind selectively to the {100} faces, leading to the formation of nanobelts showing a (100) top surface and grown along the c axis. When r was increased up to 1.5, hierarchical $BaMoO_4$ nanobelt superstructures could be formed according to a conceivable mechanism shown in Scheme 2. At 50 °C, the surfactants could preferentially bind to surfaces parallel to the [204] direction at the beginning, resulting in the formation of the [204]-oriented $BaMoO_4$ shafts. As undecylic acid was preferentially adsorbed on the crystal surfaces, the mixing ratio (r_m) between anionic and cationic surfactants in the surfactant monolayer binding to the crystal surfaces would be larger than 1.5. When the shafts grew to a certain degree, the proportion of undecylic acid in the remaining mixed surfactant film of the reverse micelles could decrease, which would result in the decrease of r to less than 1.5, leading to the growth of side nanobelts showing a (100) top surface as in the case of $r = 1.3$. Therefore, the [001]-oriented nanobelts grew continuously onto the [204]-oriented shafts with an angle of ~50°, and the penniform superstructures consisting of side nanobelts grown obliquely on the shafts formed finally. At 30 °C, the surfactants could preferentially bind to surfaces parallel to the [100] direction at the beginning, resulting in the formation of the [100]-oriented $BaMoO_4$ shafts. Similarly, on shaft growth, r would decrease to less than 1.5, leading to the final formation of the penniform superstructures consisting of

ADVANCED FUNCTIONAL MATERIALS

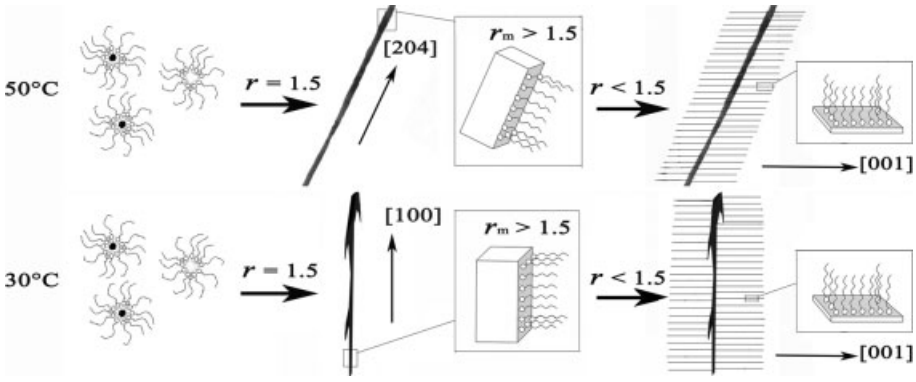

Scheme 2. Schematic illustration of the formation of hierarchical $BaMoO_4$ nanostructures at $r = 1.5$. $[BaMoO_4] = 0.05$ mol L^{-1}. r_m represents the mixing ratio between the anionic and cationic surfactants in the mixed surfactant monolayer binding to the crystal surfaces.

[001]-oriented side nanobelts grown perpendicularly on the [100]-oriented shafts. If r was further increased to $r = 1.7$, r could not be decreased to less than 1.5, even though it would decrease somewhat on shaft growth, resulting in the formation of bare shafts oriented along either the [204] direction (50 °C) or the [100] direction (30 °C).

The proposed two-stage process was supported by the observations that the formation of the shaft could be delineated from the final penniform or brush-like structures by examining the evolution process of the brushes with time. To illustrate this, the growth process of the $BaMoO_4$ brushes shown in Figure 8a, which were obtained at $r = 1.5$ after 8 h of aging at 30 °C, was followed by examining the earlier stages of their formation. As shown in Figure 10a, slightly branched, bare shafts formed at an aging time of 5 min. After 15 min of aging, nanobelts about 200 nm in length grew perpendicularly on two opposite sides of each branch (Fig. 10b). The whole growth process was very similar to that for the tree-like $BaCrO_4$ superstructures reported previously,[23] which provided evidence for a two-stage growth process. However, it should be pointed out that the proposed two-stage growth mechanism is just a tentative explanation for the experimental results and further investigation is required for a full understanding of the growth mechanism. It was noted that the growth process was accompanied by a slow precipitation process, resulting in the gradual formation of precipitates on the bottom of the solution, which indicated that the whole growth process essentially occurred in the reverse-micelle solution. Since the final penniform superstructures were usually micrometer-sized, which was significantly larger than the dimensions of individual reverse micelles, the brushes actually grew in the reverse-micelle system rather than within individual micelles, similar to the reported formation of inorganic nanowires with high aspect ratios in reverse micelles.[20] In the current situation, the formation of $BaMoO_4$ brushes may involve a continuous supply of hybrid nanoparticle precursors formed within individual micelles to the growth sites of larger crystals in the continuous medium, under the direction of the mixed surfactant molecules. This process represents another example for the mesoscale transformation of hybrid inorganic–organic building blocks into emergent nanostructures with complex form and hierarchy.[28]

It was noted that the two-stage growth mechanism could also be used to explain the formation of the penniform $BaMoO_4$ nanobelt superstructures obtained at $r = 1$ and 50 °C in the presence of PEG-*b*-PMAA. In the first stage, the polymer coupled with the catanionic surfactants induced the growth of the [100]-oriented bare shafts. Then, the catanionic surfactants with an equimolar ratio ($r = 1$) directed the growth of [001]-oriented side nanobelts, perpendicularly on the shafts.

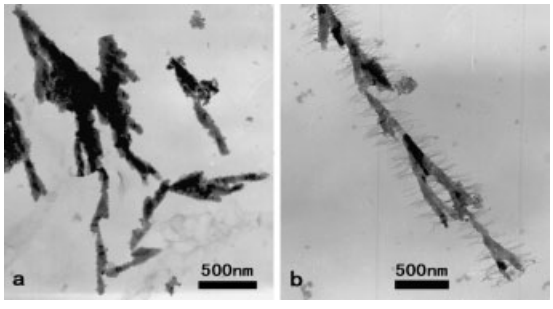

Figure 10. TEM images of BaMoO4 nanostructures obtained at earlier stages for the penniform superstructures formed at $r = 1.5$ and 30 °C. Aging time: a) 5 min, b) 15 min.

2.3. $BaWO_4$ Nanostructures

Similarly, the synthesis of $BaWO_4$ nanostructures was achieved by the reaction between Ba^{2+} ions and WO_4^{2-} ions solubilized in catanionic reverse micelles. As reported in a recent communication,[22] bundles of [001]-oriented $BaWO_4$ nanowires with diameters of ~3.5 nm and lengths larger than 50 μm were produced in the catanionic reverse micelles at $r = 1$ and 50 °C (Figs. 11a,b). At this reaction temperature, $BaWO_4$ nanobelts with lengths up to several tens of micrometers, widths of ~20 nm, and thickness of ~4 nm were obtained at $r = 0.6$ (Figs. 11c,d). The related HRTEM image (Fig. 11e) suggested that the nanobelts were $BaWO_4$ single crystals grown along the [001] direction. The XRD pattern and the XPS spectra shown in Figure 12 confirmed that the products were pure $BaWO_4$ crystals of a tetragonal scheelite structure (JCPDS card 43-0646: $a = 0.561$ nm, $c = 1.270$ nm). At $r = 1.2$, a value slightly larger than 1, similar $BaWO_4$ nanobelts were obtained and the related ED pattern indicated that the nanobelts were grown along the [001] direction with the top (100) surface (Fig. 11f).

When r was increased to 1.35, penniform architectures consisting of [001]-oriented $BaWO_4$ nanobelts grown perpendicularly

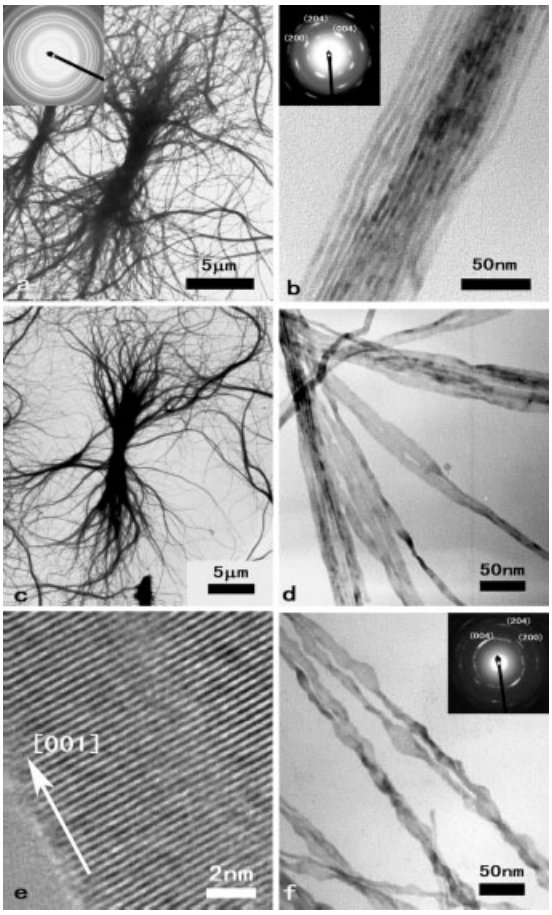

Figure 11. a–d,f) TEM and e) HRTEM images of $BaWO_4$ nanostructures formed at 50 °C and $r = 1$ (a,b), 0.6 (c–e), and 1.2 (f). $[BaWO_4]$ = 0.025 mol L^{-1}. Insets show the corresponding ED patterns. (Figures a and b from [22] reproduced by permission of The Royal Society of Chemistry, Copyright 2002).

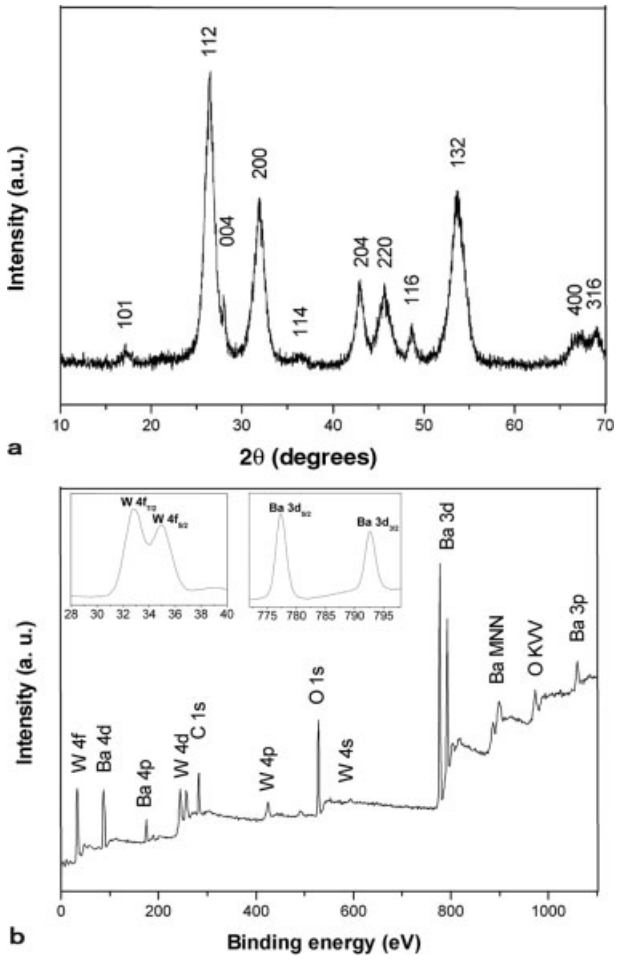

Figure 12. a) XRD pattern and b) XPS spectra of $BaWO_4$ nanobelts formed at $r = 0.6$ and 50 °C. $[BaWO_4] = 0.025$ mol L^{-1}.

on both sides of the [100]-oriented shafts were produced (Fig. 13a). The enlarged image (Fig. 13b) indicated that most of the side nanobelts were aligned face to face with the top surface, perpendicular to the shaft direction, i.e., the *a* axis. However, side nanobelts grown with the top surface parallel to the shaft direction were occasionally observed, as indicated by the arrow in Fig. 13b. As the (100) and (010) surfaces are actually equivalent crystal surfaces belonging to the {100} surfaces of the tetragonal structure, it would be rational that the [001]-oriented side nanobelts were grown with their top surface randomly perpendicular or parallel to the shaft direction. The interaction between the hydrophobic tails of the surfactants adsorbed on the crystal surfaces would largely contribute to the parallel alignment of the nanobelts, face to face, rather than face to edge or edge to edge. It was expected that such a face-to-face alignment might be further favored at a higher density of nanobelt arrays. This was confirmed by the observation that almost all the side nanobelts were aligned face to face for the penniform $BaWO_4$ nanostructures with more dense nanobelts arrays, which were obtained under the same conditions except for a higher reactant concentration (Figs. 13c,d). A schematic illustration of the alignment of the side nanobelts along the shaft of the penniform nanostructures is presented in Scheme 3. When r was further increased to 1.5, bare $BaWO_4$ shafts grown along the [100] direction could be obtained, very similar to the bare $BaMoO_4$ shafts obtained at $r = 1.7$.

The obvious similarity in the architectural changes of the $BaMoO_4$ and $BaWO_4$ nanostructures with increasing r strongly indicated that the formation of penniform $BaWO_4$ nanobelt superstructures followed the two-stage growth mechanism proposed for hierarchical $BaMoO_4$ nanostructures. The two-stage growth mechanism was supported by the reported formation of penniform $BaWO_4$ nanowire superstructures, obtained in catanionic reverse micelles at $r = 1$ in the presence of PEG-*b*-PMAA.[12] In this case, the polymer coupled with the catanionic surfactants first induced the growth of the [100]-oriented bare shafts. Then, the equimolar surfactant mixture ($r = 1$) directed the growth of [001]-oriented side nanowires (rather than nanobelts) perpendicularly on the shafts, since the formation of $BaWO_4$ nanowires was favored in catanionic reverse micelles at $r = 1$. Moreover, our preliminary experimental results showed that in the presence of PEG-*b*-PMAA, penniform

ADVANCED FUNCTIONAL MATERIALS

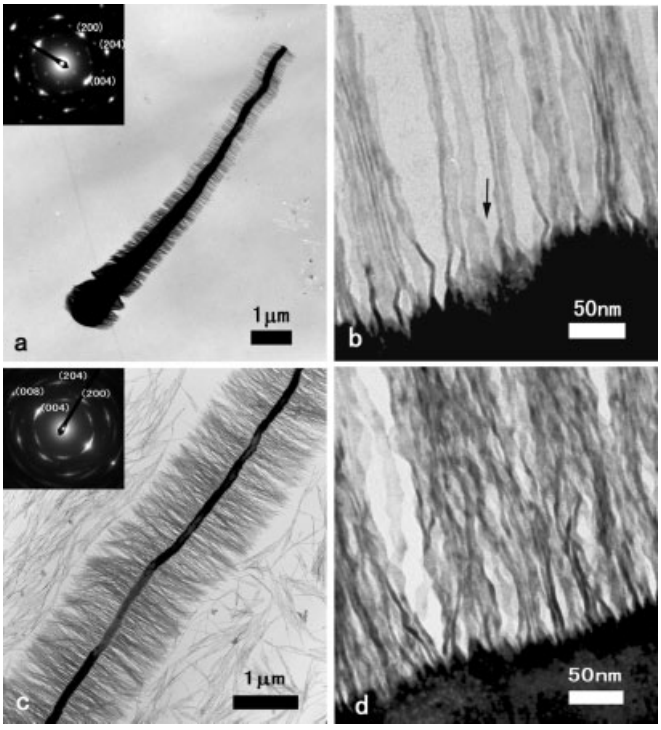

Figure 13. TEM images of $BaWO_4$ nanostructures formed at $r = 1.35$ and 50 °C. [$BaWO_4$]: a,b) 0.025 mol L^{-1}, c,d) 0.1 mol L^{-1}. Insets show the corresponding ED patterns.

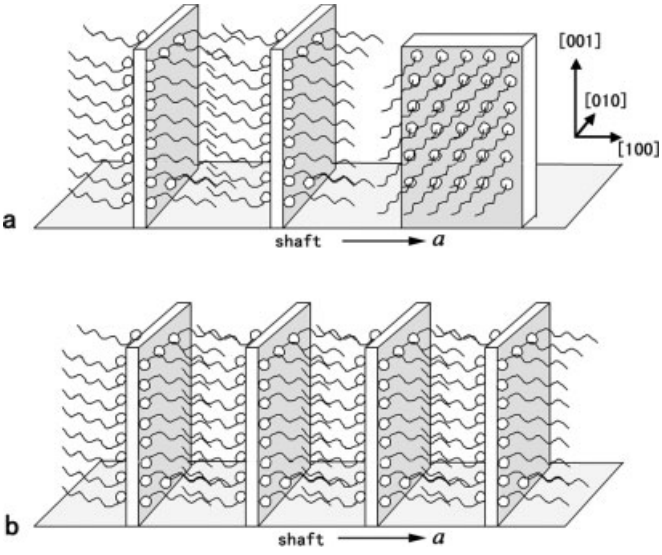

Scheme 3. Schematic illustration of the alignment of the side nanobelts of the penniform $BaWO_4$ nanobelt superstructures formed at $r = 1.35$ and 50 °C. [$BaWO_4$]: a) 0.025 mol L^{-1}, b) 0.1 mol L^{-1}.

$BaWO_4$ nanobelt superstructures were obtained at $r = 1.2$ where the formation of $BaWO_4$ nanobelts was favored, which provided further support for the two-stage growth mechanism.

It is worth noting that there existed some differences between the cases of $BaMoO_4$ and $BaWO_4$. First, it seemed that $BaMoO_4$ had a strong tendency to form nanobelts whereas $BaWO_4$ tended to form nanowires in catanionic reverse micelles at $r = 1$. Second, the shaft of the penniform $BaMoO_4$ nanostructures adopted two different crystal directions, i.e., the [204] and [100] directions depending on the reaction temperature, whereas the shaft of the penniform $BaWO_4$ nanostructures adopted just one crystal direction, i.e., the [100] direction. It is known that both $BaMoO_4$ and $BaWO_4$ crystals have a tetragonal scheelite structure with similar unit cell parameters (for $BaMoO_4$, $a = 0.558$ nm, $c = 1.282$ nm; for $BaWO_4$, $a = 0.561$ nm, $c = 1.270$ nm). Therefore, the lattice-matching model is hardly applicable for the explanation of the selective adsorption of surfactants on the $BaMoO_4/BaWO_4$ crystal surfaces. Currently, the real reason for the differences is still unclear; however, it is believed that the inherent growth habit of the crystals, as well as the specific interaction between the surfactants and the crystal surfaces may have played an important role.

3. Conclusion

$BaMoO_4$ and $BaWO_4$ nanobelts and a variety of hierarchical superstructures assembled from the nanobelts have been synthesized in a catanionic reverse-micelle system formed by undecylic acid and decyl amine. Architectural control of the hierarchical nanobelt superstructures has been readily achieved by changing the experimental parameters. At a suitable surfactant mixing ratio ($r = 1.5$), two different kinds of penniform $BaMoO_4$ nanobelt superstructures, i.e., one consisting of [001]-oriented nanobelts grown obliquely on a [204]-oriented shaft and the other consisting of [001]-oriented nanobelts grown perpendicularly on a [100]-oriented shaft, were produced at 50 °C and 30 °C, respectively. Penniform $BaWO_4$ nanobelt superstructures consisting of [001]-oriented nanobelts grown perpendicularly on a [100]-oriented shaft were also produced at a suitable surfactant mixing ratio ($r = 1.35$). A plausible two-stage growth mechanism has been proposed for the formation of penniform $BaXO_4$ nanobelt superstructures in catanionic reverse micelles. Such catanionic reverse-micelle systems may represent promising nanostructured media for the solution synthesis of inorganic nanobelts and their hierarchical assembly into complex nanobelt superstructures.

4. Experimental

Materials: Undecylic acid (99 %, Aldrich), decyl amine (95 %, Aldrich), and poly(ethylene glycol)-*block*-poly(methacrylic acid) (PEG-*b*-PMAA, PEG = 3000 g mol^{-1}, PMAA = 700 g mol^{-1}, Goldschmidt AG) were used as received. Decane (95 %, Beijing Chemical Reagents Co.) was distilled once before use. Na_2MoO_4, Na_2WO_4, and $BaCl_2$ were of analytical grade and supplied by Beijing Chemical Reagent. The water used was deionized.

Synthesis of $BaXO_4$ Nanostructures: Undecylic acid and decyl amine were mixed in the liquid state under mild heating, leading to the production of a catanionic surfactant mixture, which was a white solid at room temperature. The synthesis of $BaXO_4$ nanostructures was simply achieved by the reaction of the corresponding reactant ions solubilized in the catanionic micelles. In a typical synthesis of $BaMoO_4$ nanostruc-

tures, the catanionic surfactant mixture (0.782 g) was first dissolved in decane (2.5 mL) under mild heating. Then, a 0.1 mol L^{-1} Na_2MoO_4 solution (100 μL) was added with shaking, which was followed by the addition of 0.1 mol L^{-1} $BaCl_2$ (100 μL) and vigorous shaking, giving a reactant concentration of 0.05 mol L^{-1} with respect to the aqueous phase of the reverse micelles. Finally, the resultant mixture was incubated for 8 h at temperatures ranging from 30 to 50 °C, resulting in the formation of white precipitates.

Characterization: The products were collected, washed with ethanol, and characterized using transmission electron microscopy (TEM, JEOL JEM-200CX), high-resolution transmission electron microscopy (HRTEM, Tecnai F30), X-ray diffraction (XRD, Rigaku Dmax-2000 with Cu Kα radiation), and X-ray photoelectron spectroscopy (XPS, Kratos Axis Ultra spectrometer with monochromized Al Kα radiation).

Received: June 4, 2004
Final version: September 2, 2004

[1] a) J. Hu, T. W. Odom, C. M. Lieber, *Acc. Chem. Res.* **1999**, *32*, 435. b) G. R. Patzke, F. K. Krumeich, R. Nesper, *Angew. Chem. Int. Ed.* **2002**, *41*, 2446. c) Y. Xia, P. Yang, Y. Sun, Y. Wu, B. Mayers, B. Gates, Y. Yin, F. Kim, H. Yan, *Adv. Mater.* **2003**, *15*, 353. d) C. N. R. Rao, F. L. Deepak, G. Gundiah, A. Govindaraj, *Prog. Solid State Chem.* **2003**, *31*, 5.

[2] M. Li, H. Schnablegger, S. Mann, *Nature* **1999**, *402*, 393.

[3] a) L. Manna, D. J. Milliron, A. Meidel, E. C. Scher, A. P. Alivisatos, *Nat. Mater.* **2003**, *2*, 382. b) D. Wang, C. M. Lieber, *Nat. Mater.* **2003**, *2*, 355.

[4] N. I. Kovtyukhova, T. E. Mallouk, *Chem. Eur. J.* **2002**, *8*, 4354.

[5] Y. Wu, H. Yan, M. Huang, B. Messer, J. H. Song, P. Yang, *Chem. Eur. J.* **2002**, *8*, 1260.

[6] E. Dujardin, L.-B. Hsin, C. R. C. Wang, S. Mann, *Chem. Commun*. **2001**, 1264.

[7] a) F. Kim, S. Kwan, J. Akana, P. Yang, *J. Am. Chem. Soc.* **2001**, *123*, 4360. b) P. Yang, F. Kim, *ChemPhysChem* **2002**, *3*, 503. c) D. Whang, S. Jin, Y. Wu, C. M. Lieber, *Nano Lett.* **2003**, *3*, 1255.

[8] a) X. Wang, C. J. Summers, Z. L. Wang, *Nano Lett*. **2004**, *4*, 423. b) E. C. Walter, M. P. Zach, F. Favier, B. J. Murray, K. Inazu, J. C. Hemminger, R. M. Penner, *ChemPhysChem* **2003**, *4*, 131.

[9] a) J. Y. Lao, J. G. Wen, Z. F. Ren, *Nano Lett.* **2002**, *2*, 1287. b) J. Y. Lao, J. Y. Huang, D. Z. Wang, Z. F. Ren, *Nano Lett.* **2003**, *3*, 235. c) H. Yan, R. He, J. Johnson, M. Law, R. J. Saykally, P. Yang, *J. Am. Chem. Soc.* **2003**, *125*, 4728.

[10] a) Z. A. Peng, X. Peng, *J. Am. Chem. Soc.* **2002**, *124*, 3343. b) Y. Jun, Y. Jing, J. Cheon, *J. Am. Chem. Soc.* **2002**, *124*, 615. c) S. Chen, Z. L. Wang, J. Ballato, S. H. Foulger, D. L. Carroll, *J. Am. Chem. Soc.* **2003**, *125*, 16 186.

[11] a) L. Qi, H. Cölfen, M. Antonietti, M. Li, J. D. Hopwood, A. J. Ashley, S. Mann, *Chem. Eur. J.* **2001**, *7*, 3526. b) S. H. Yu, M. Antonietti, H. Cölfen, J. Hartmann, *Nano Lett.* **2003**, *3*, 379.

[12] H. Shi, L. Qi, J. Ma, H. Cheng, *J. Am. Chem. Soc.* **2003**, *125*, 3450.

[13] Q. Lu, F. Gao, S. Komarneni, *J. Am. Chem. Soc.* **2004**, *126*, 54.

[14] a) Z. W. Pan, Z. R. Dai, Z. L. Wang, *Science* **2001**, *291*, 1947. b) X. Y. Kong, Y. Ding, R. Yang, Z. L. Wang, *Science* **2004**, *303*, 1348. c) C. Ma, D. Moore, J. Li, Z. L. Wang, *Adv. Mater.* **2003**, *15*, 228. d) Z. R. Dai, Z. W. Pan, Z. L. Wang, *Adv. Funct. Mater.* **2003**, *13*, 9.

[15] S.-H. Yu, M. Antonietti, H. Cölfen, M. Giersig, *Angew. Chem. Int. Ed.* **2002**, *114*, 2462.

[16] P. Gao, Z. L. Wang, *J. Phys. Chem. B* **2002**, *106*, 12 653.

[17] M.-P. Pileni, *Nat. Mater.* **2003**, *2*, 145.

[18] a) M. P. Pileni, *Langmuir* **2001**, *17*, 7476. b) J. Zhang, B. Han, M. Liu, D. Liu, Z. Dong, J. Liu, D. Li, *J. Phys. Chem. B* **2003**, *107*, 3679.

[19] B. A. Simmons, S. Li, V. T. John, G. L. McPherson, A. Bose, W. Zhou, J. He, *Nano Lett.* **2002**, *2*, 263.

[20] a) L. Qi, J. Ma, H. Cheng, Z. Zhao, *J. Phys. Chem. B* **1997**, *101*, 3460. b) J. D. Hopwood, S. Mann, *Chem. Mater.* **1997**, *9*, 1819. c) M. Li, S. Mann, *Langmuir* **2000**, *16*, 7088. d) S. Kwan, F. Kim, J. Akana, P. D. Yang, *Chem. Commun.* **2001**, 447.

[21] a) X. Peng, L. Manna, W. Yang, J. Wickham, E. Scher, A. Kadavanich, A. P. Alivisatos, *Nature* **2000**, *404*, 59. b) V. F. Puntes, K. M. Krishnan, A. P. Alivisatos, *Science* **2001**, *291*, 2115. c) Y. Jun, M. F. Casula, J.-H. Sim, S. Y. Kim, J. Cheon, A. P. Alivisatos, *J. Am. Chem. Soc.* **2003**, *125*, 15 981. d) F. Dumestre, B. Chaudret, C. Amiens, M. Respaud, P. Fejes, P. Renaud, P. Zurcher, *Angew. Chem. Int. Ed.* **2003**, *42*, 5213.

[22] H. Shi, L. Qi, J. Ma, H. Cheng, *Chem. Commun.* **2002**, 1704.

[23] H. Shi, L. Qi, J. Ma, H. Cheng, B. Zhu, *Adv. Mater.* **2003**, *15*, 1647.

[24] a) S.-H. Yu, B. Liu, M.-S. Mo, J.-H. Huang, X.-M. Liu, Y.-T. Qian, *Adv. Funct. Mater.* **2003**, *13*, 639. b) X. Cui, S.-H. Yu, L. Li, L. Biao, H. Li, M. Mo, X.-M. Liu, *Chem. Eur. J.* **2004**, *10*, 218. c) Y. Xiong, Y. Xie, Z. Li, X. Li, S. Gao, *Chem. Eur. J.* **2004**, *10*, 654.

[25] a) J. Bi, D. Q. Xiao, D. J. Gao, P. Yu, G. L. Yu, W. Zhang, J. G. Zhu, *Cryst. Res. Technol.* **2003**, *38*, 935. b) B. Xie, Y. Wu, Y. Jiang, F. Li, J. Wu, S. Yuan, W. Yu, Y. Qian, *J. Cryst. Growth* **2002**, *235*, 283. c) P. Černý, H. Jelínková, *Opt. Lett.* **2002**, *27*, 360.

[26] B.-Y. Zhu, H.-T. Shi, J.-B. Huang, X. He, *Acta Chim. Sin.* **2001**, *59*, 913.

[27] B. Jönsson, P. Jokela, A. Khan, B. Lindman, A. Sadaghiani, *Langmuir* **1991**, *7*, 889.

[28] H. Cölfen, S. Mann, *Angew. Chem. Int. Ed.* **2003**, *42*, 2350.

